Photoacoustic frequency-domain depth profiling of continuously inhomogeneous condensed phases: Theory and simulations for the inverse problem

Andreas Mandelis[a] and Samuel B. Peralta
Photoacoustic and Photothermal Sciences Laboratory and Ontario Laser and Lightwave Research Center, Department of Mechanical Engineering, University of Toronto, Toronto M5S 1A4, Canada

Jan Thoen
Laboratorium voor Akoestiek en Warmtegeleiding, Department of Physics, Katholieke Universiteit Leuven, B-3001 Leuven, Belgium

(Received 8 February 1991; accepted for publication 2 May 1991)

An application is presented of the Hamilton–Jacobi formulation of thermal-wave physics [A. Mandelis, J. Math. Phys. **26**, 2676 (1985)] to the problem of photoacoustic depth profiling of inhomogeneous solids with arbitrary, continuously varying thermal diffusivity profiles. Simple expressions for the modulation frequency dependence of the photoacoustic signal in the case of exponential thermal diffusivity profiles are obtained, and a working general method for solving the inverse problem and obtaining arbitrary diffusivity depth profiles is demonstrated through computer simulations. The method was found to possess excellent profile reconstruction fidelity.

I. INTRODUCTION

Photoacoustic depth profiling of inhomogeneous solids is a most important manifestation of the nondestructive evaluation (NDE) capabilities of this technique. Even though much experimental work[1–4] and some theoretical models[2,5] have been published with discontinuously inhomogeneous solids, theoretical implementation of realistic models addressing the equally important, and frequently more common, problem of continuously inhomogeneous solids has been less fertile. Afromowitz *et al.*[6] and Harata and Sawada[7] have treated the problem of a solid with spatially continuously varying optical absorption coefficient and constant thermal properties. In both treatments a signal inversion based on the spatial Laplace transform of the photoacoustic frequency response of the sample yielded approximate depth profiles of the optical absorption coefficient. Unfortunately, the same convenient Laplace transform formulation cannot be applied to the case of solids with continuously varying thermal/thermodynamic parameters (thermal conductivity, specific heat, density); yet, this class of materials is encountered much more commonly in nondestructive evaluation applications than the optically continuously inhomogeneous solids. Approximate formulations of this thermal-wave problem have been presented in the form of series expansions for specific thermal conductivity profiles and constant specific heat and sample density by Thakur.[8] However, the complexity of the final expressions for each profile and the lack of a criterion for the parameter ranges within which the infinite series expansions are well behaved may be an obstacle in the direct use of these expressions with photoacoustic data. Thakur further presented[8] an integral formulation of the same problem based on the Wentzel–Kramers–Brillouin–Jeffreys (WKBJ) approximation[9] and valid for slowly varying thermal conductivity profiles, a somewhat restrictive assumption. Perturbation types of expansions for the thermal conductivity, $k_s(x)$, and specific heat, $c_s(x)$, about their surface values, $k_s(0)$ and $c_s(0)$, have been assumed for slightly inhomogeneous solids by Gusev *et al.*[10] First-order regular perturbation theory was then used to obtain expressions for the thermal-wave field, but no attempt was made to invert the photoacoustic response. The most general and rigorous approach to the inverse thermal-wave problem has been given by Vidberg *et al.*[11] These workers addressed the rather special situation of thermal-wave surface signals obtained by measuring the radial variation of the surface temperature of a continuously inhomogeneous solid about a heated point at a single modulation frequency. Both thermal conductivity and heat capacity profiles were reconstructed using Padé approximants for the inversion of spatial Laplace transforms; however, several constraints accompany the technique of Vidberg *et al.* The most important ones are the nonconventional experimental geometry for which it is only valid: the fact that the theoretical problem is ill-posed and thus the reconstructed profiles are not always numerically reliable; the limitation of the accuracy to a depth reconstruction on the order of one thermal diffusion length; and the relative complexity of the reconstruction algorithm, as well as its acute sensitivity to the presence of small amounts of error ($\sim 2\%$, i.e., within a normal experimental standard deviation), which seem to yield a significantly altered heat capacity reconstruction profile. The same group[12] had previously presented a numerical analysis of the same geometry based on the solution of the thermal-wave equation, at a single modulation frequency, via a two-dimensional finite difference grid.

[a]On leave at Laboratorium voor Akoestiek en Warmtegeleiding, Dept. of Physics, Katholieke Univ. Leuven, Belgium.

 0021-8979/91/031761-10$03.00

Thermal-wave phase-derived diffusivity profiles were thus obtained for surface-hardened steel.

In this work we have addressed the depth-profiling thermal-wave problem for continuously thermally varying solids in the conventional frequency-domain microphone-based photoacoustic spectrometry (PAS). Unlike the earlier treatments, well-posed, direct, simple and convenient expressions for the frequency dependence of the PA signal are obtained based on the classical mechanical concept of the Hamilton–Jacobi thermal harmonic oscillator (THO).[13] Simple analytical inversions of simulated amplitude and phase data can yield thermal diffusivity spatial profiles by means of a self-adjusting method based on the experimental modulation frequency response of optically opaque continuously inhomogeneous samples; this method renders the diffusivity profile reconstruction largely independent of assumed specific mathematical profiles.

II. THEORY

A. The Hamilton–Jacobi THO

It has been shown[13] that the temperature field

$$\theta(x,t)=T(x)\exp(i\omega t), \tag{1a}$$

i.e., the solution to the thermal-wave equation

$$\frac{\partial}{\partial x}\left(k(x)\frac{\partial}{\partial x}\theta(x,t)\right)-\rho(x)c(x)\frac{\partial}{\partial t}\theta(x,t)=0 \tag{1b}$$

in a semi-infinite solid medium with continuously variable thermal conductivity, $k(x)$, density, $\rho(x)$, and specific heat, $c(x)$, which is excited by a photothermal source at an intensity modulation angular frequency, ω, gives rise to a thermal harmonic oscillator (THO) field with the classical canonical Hamiltonian function:

$$H(\tau,p_\tau)=\frac{1}{2m}p_\tau^2+\frac{1}{2}K\tau^2, \tag{2}$$

where the following generalized functions are defined:

$$\tau\equiv[k(x)\rho(x)c(x)]^{1/4}T(x);\ \text{(position)} \tag{3}$$

$$p_\tau\equiv -k(x)\frac{dT(x)}{dx};\ \text{(momentum)} \tag{4}$$

$$m^{-1}\equiv\lim_{L\to\infty}\left(\frac{1}{L}\int_0^L\frac{dy}{\sqrt{\alpha_s(y)}}\right);\ \text{(inertia)} \tag{5}$$

$$K\equiv -i\omega m^{-1};\ \text{(spring constant)}, \tag{6}$$

and

$$\alpha_s(x)\equiv k(x)/\rho(x)c(x) \tag{7}$$

is the thermal diffusivity of the solid at depth x from the surface ($x=0$). The THO Hamiltonian is a constant of the motion[14] and assumes the meaning of the total generalized energy E of the thermal-wave field:

$$\frac{1}{2m}\left(\frac{\partial W}{\partial\tau}\right)^2+\frac{K}{2}\tau^2=c_1\equiv E, \tag{8}$$

where $W(\tau,c_1)$ is Hamilton's characteristic function, related to the principal function $S(\tau,\zeta,c_1)$ through[14]

$$S(\tau,\zeta,c_1)=W(\tau,c_1)-c_1\zeta \tag{9}$$

and

$$\zeta\equiv m\int_0^x\frac{dy}{\sqrt{\alpha_s(y)}}. \tag{10}$$

Equations (8) and (9) give

$$S(\tau,\zeta,c_1)=\sqrt{mK}\int\left(\frac{2c_1}{K}-\tau^2\right)^{1/2}d\tau-c_1\zeta \tag{11}$$

so that the constant ψ may be defined[14]

$$\psi\equiv\frac{\partial S}{\partial c_1}=\sqrt{\frac{m}{K}}\sin^{-1}\left(\sqrt{\frac{K}{2c_1}}\tau\right)-\zeta. \tag{12}$$

Upon defining the THO angular spatial frequency

$$\Omega_\tau\equiv(K/m)^{1/2}=ie^{i\pi/4}\sqrt{\omega}/m, \tag{13}$$

Eq. (12) yields

$$\tau(\zeta)=\left(\frac{2c_1}{K}\right)^{1/2}\sin\left(ie^{i\pi/4}\frac{\sqrt{\omega}}{m}(\zeta+\psi)\right) \tag{14}$$

subject to an initial condition obtained from Eq. (11):

$$p_\tau(x=0)=\left.\frac{\partial S}{\partial\tau}\right|_{\tau=\tau_0}=\sqrt{2m}\left(c_1-\frac{1}{2}K\tau_0^2\right)^{1/2}. \tag{15}$$

Letting the thermal flux (momentum) at the surface $x=0$ be Q_0, Eq. (14) gives an expression for c_1:

$$c_1=\frac{1}{2m}Q_0^2+\frac{1}{2}m\Omega_\tau^2\tau_0^2. \tag{16}$$

For simplicity and in analogy with the classical mechanical harmonic oscillator, we assume that the flux term at the surface is associated with exactly half the total energy $c_1=E$ of the THO; the other half is contributed by the term proportional to the boundary temperature:

$$\tau_0\propto T(0). \tag{17}$$

Now, Eq. (14) may be written as

$$\tau(\zeta)=\tau_0\sinh\left(e^{i\pi/4}\frac{\sqrt{\omega}}{m}(\zeta+\psi)\right), \tag{18}$$

where

$$e^{i\pi/4}\frac{\sqrt{\omega}}{m}\zeta=\int_0^x\sigma(y,\omega)dy\equiv H(x) \tag{19}$$

and $\sigma(y,\omega)$ is the depth-dependent complex thermal diffusion coefficient[13,15]

$$\sigma(y,\omega)\equiv(1+i)[\omega/2\alpha_s(y)]^{1/2}. \tag{20}$$

Finally, expanding the hyperbolic sine term of Eq. (18) in terms of exponentials and noting that

$$e^{i\pi/4}\frac{\sqrt{\omega}}{m}\psi=\lim_{L\to\infty}\left(\frac{1}{L}\int_0^L\sigma(y,\omega)dy\right)\psi$$
$$=\langle\sigma(\omega)\rangle\psi=\text{constant},$$

one may write for the temperature field $T(x)$, Eq. (3):

$$T(x)=T(0)\left(\frac{e_s(0)}{e_s(x)}\right)^{1/2}[C_1e^{H(x)}-C_2e^{-H(x)}], \quad (21)$$

where C_1, C_2 are integration constants to be determined from boundary conditions, and

$$e_s(x)=[k(x)\rho(x)c(x)]^{1/2} \quad (22)$$

is the material thermal effusivity.

B. Solids with constant and finite optical absorption coefficient β: Continuously inhomogeneous thermal properties

Considering Eq. (21) as the (complementary) solution to the homogeneous thermal-wave problem, Eq. (2), it is straightforward to approach the solution to the inhomogeneous problem:[15]

$$\frac{d}{dx}\left(k(x)\frac{d}{dx}T(x)\right)-i\omega\rho(x)c(x)T(x)$$
$$=-\frac{1}{2}\eta\beta I_0\exp(\beta x); \quad x<0, \quad (23)$$

where $\eta(\lambda)$ is the nonradiative (optical-to-thermal) conversion efficiency, $\beta(\lambda)$ is the constant optical absorption coefficient, and I_0 is the amplitude of the modulated optical intensity incident on the sample surface. Assuming a particular solution of Eq. (23) of the form

$$T_p(x)=F(x)\left(\frac{\exp[H(x)]}{\sqrt{e_s(x)/e_s(0)}}\right)+G(x)\left(\frac{\exp[-H(x)]}{\sqrt{e_s(x)/e_s(0)}}\right), \quad (24)$$

subject to

$$\frac{dF(x)}{dx}\exp[H(x)]+\frac{dG(x)}{dx}\exp[-H(x)]=0, \quad (25)$$

and making the approximation

$$\frac{d}{dx}[k(x)c(x)\rho(x)]^{-1/4}\approx 0\left(\text{i.e., }\frac{d}{dx}e_s^{-1/2}(x)\approx 0\right), \quad (26)$$

one finds

$$\frac{dF(x)}{dx}=-\frac{1}{2}Q_0\frac{\beta e^{\beta x}}{k(x)\sigma(x)}\left(\frac{e_s(x)}{e_s(0)}\right)^{1/2}e^{-H(x)} \quad (27a)$$

and

$$\frac{dG(x)}{dx}=\frac{1}{2}Q_0\frac{\beta e^{\beta x}}{k(x)\sigma(x)}\left(\frac{e_s(x)}{e_s(0)}\right)^{1/2}e^{H(x)}, \quad (27b)$$

where

$$Q_0\equiv\tfrac{1}{2}\eta I_0. \quad (28)$$

The complete solution for the inhomogeneous thermal-wave problem is given from Eqs. (21), (24), (27):

$$T(x)=\left(C_1-\frac{1}{2}Q_0\beta\int_0^x\exp[\beta x'-H(x')]\times\frac{E^{1/2}(x')dx'}{k(x')\sigma(x')}\right)\frac{\exp[H(x)]}{E^{1/2}(x)}$$
$$-\left(C_2-\frac{1}{2}Q_0\beta\int_0^x\exp[\beta x'+H(x')]\times\frac{E^{1/2}(x')dx'}{k(x')\sigma(x')}\right)\frac{\exp[-H(x)]}{E^{1/2}(x)}, \quad (29)$$

where we defined

$$E(x)\equiv e_s(x)/e_s(0) \quad (30)$$

and the constant $T(0)$ in Eq. (21) was absorbed in the constants C_1 and C_2. For a semi-infinite solid in thermal contact with a semi-infinite carrier gas, as in a photoacoustic cell, the boundary conditions are:

(i) For $x\to-\infty$, $T(x)\to 0$, i.e., $e^{-H(x)}\to\infty$, which requires

$$C_2=-\frac{1}{2}Q_0\beta\int_{-\infty}^0\exp[\beta x'+H(x')]\frac{E^{1/2}(x')dx'}{k(x')\sigma(x')}. \quad (31)$$

(ii) At $x=0$ (interface) and assuming for the gas[15]

$$T_g(x)=\theta_g e^{-\sigma_g x}, \quad (32)$$

where

$$\sigma_g\equiv(1+i)(\omega/2\alpha_g)^{1/2}, \quad (33)$$

continuity of temperature requires

$$C_1-C_2=\theta_g \quad (34)$$

and continuity of heat flux requires

$$C_1+C_2=-g\theta_g;\ g\equiv\frac{k_g\sigma_g}{k(0)\sigma(0)}. \quad (35)$$

Therefore,

$$C_1=-\left(\frac{1-g}{1+g}\right)C_2 \quad (36)$$

and Eqs. (29) and (32) give, respectively:

$$T(x)=\frac{1}{2}Q_0\beta\left\{\left[\left(\frac{1-g}{1+g}\right)\int_{-\infty}^0\exp[\beta x'+H(x')]\times\frac{E^{1/2}(x')dx'}{k(x')\sigma(x')}+\int_x^0\exp[\beta x'-H(x')]\times\frac{E^{1/2}(x')dx'}{k(x')\sigma(x')}\right]\frac{\exp[H(x)]}{E^{1/2}(x)}+\left(\int_{-\infty}^x\exp[\beta x'+H(x')]\frac{E^{1/2}(x')dx'}{k(x')\sigma(x')}\right)\frac{\exp[-H(x)]}{E^{1/2}(x)}\right\};\ x<0 \quad (37)$$

and

$$T_g(x)=\frac{Q_0\beta}{1+g}\left(\int_{-\infty}^{0}\exp[\beta x'+H(x')]\times\frac{E^{1/2}(x')dx'}{k(x')\sigma(x')}\right)e^{-\sigma_g x};\quad x\geqslant 0. \tag{38}$$

In the special case where $k(x)$, $\rho(x)$, and $c(x)$ are constant and not functions of depth, Eqs. (37) and (38) yield

$$T(x)=\frac{\eta\beta I_0}{2k(\beta^2-\sigma^2)}\left[\left(\frac{g+r}{g+1}\right)e^{\sigma x}-e^{\beta x}\right];\quad x\leqslant 0 \tag{39}$$

and

$$T_g(x)=\frac{\eta\beta I_0}{2k(\beta^2-\sigma^2)}\left(\frac{r-1}{g+1}\right)e^{-\sigma_g x};\quad x\geqslant 0 \tag{40}$$

where $r\equiv\beta/\sigma$. Equations (39) and (40) are precisely those obtained by the Rosencwaig–Gersho (RG) model[15] in the limit of semi-infinite solid and gas.

Since our main interest in this theory is in its application to the simpler case of photoacoustically saturated[15] condensed phase media, such as strongly absorbing liquid crystals,[16] the full Eqs. (37) and (38) will not be considered further here; however, the only approximation (26) will be taken up again in Section IV.

C. Condensed phase media in the photoacoustic saturation regime: Continuously inhomogeneous thermal properties

We are interested in the exact homogeneous solution, Eq. (21), subject to appropriate boundary conditions for photoacoustically saturated media. The heat flux at any depth x may be written:

$$F(x)=-k(x)\frac{d}{dx}T(x)$$

$$=\frac{-T(0)}{E^{1/2}(x)}k(x)\sigma(x)[C_1e^{H(x)}+C_2e^{-H(x)}], \tag{41}$$

where a second term has been omitted, assumed negligible compared to the term above. This approximation amounts, as before, to

$$\frac{d}{dx}e_s^{-1/2}(x)\approx 0. \tag{26}$$

One boundary condition for semi-infinite media is

$$\lim_{x\to\infty}T(x)=0\Rightarrow C_1=C_2e^{-2H(\infty)}. \tag{42}$$

The other condition pertains to the thermal flux as $x\to\infty$ and depends on the general functional dependence, $\alpha_s=\alpha_s(x)$, of the thermal diffusivity: for monotonically decreasing $\alpha_s(x)$, as $x\to\infty$ the flux must be equal to that resulting from a linear superposition of a homogeneous medium with $\alpha_s=\alpha_s(\infty)\equiv\alpha_\infty<\alpha_s(x)$, plus a contribution due to the excess flux of the higher diffusivity medium:

$$F(x\to\infty)=\tfrac{1}{2}\{F(x\to\infty;\alpha_\infty)+\Delta F[x\to\infty;\alpha_s(x)]\}. \tag{43}$$

The factor 1/2 appears in order to account for adding twice the fluxes from the medium with $\alpha_s=\alpha_\infty$ plus that with $\alpha_s=\alpha_\infty+\Delta\alpha$. Furthermore, the term ΔF may be written as a fraction of the flux at $x=0$, where $\alpha_s=\alpha_s(0)\equiv\alpha_0>\alpha_s(x)$. This fraction is set equal to f_{x0} and remains to be determined from the prescribed value of Eq. (21) at $x=0$. With Q_0 being the thermal energy flux at the surface, Eq. (28), the second boundary condition must be expressed as a limit-taking process:

$$\lim_{x\to\infty}F(x)=\frac{Q_0}{2}\lim_{x\to\infty}[e^{-\sigma_\infty x}+f_{x0}e^{-H(x)}]. \tag{44}$$

In the limit $x=0$ in Eq. (21), letting $T(0)$ be interpreted as the surface temperature of the condensed medium with homogeneous $\alpha_s=\alpha_0$ profile due to the incident flux Q_0, we obtain[13,17]

$$T(0)=Q_0/k_0\sigma_0\equiv T_0(\omega). \tag{45}$$

Equations (41), (42), (44) yield

$$C_2=-\frac{1}{4}R^{1/2}(\infty)\lim_{x\to\infty}\{\exp[-\sigma_\infty x+H(x)]+f_{x0}\exp[-H(x)+H(\infty)]\};\quad \alpha_0>\alpha_\infty \tag{46a}$$

where

$$R(x)\equiv E^{-1}(x)=e_s(0)/e_s(x). \tag{46b}$$

The form of C_2 will only be determined by the specific functional dependence $\alpha_s=\alpha_s(x)$, as it is contained in the integral $H(x)$.

In the case of monotonically increasing $\alpha_s(x)$, as $x\to\infty$ the second boundary condition for $F(x\to\infty)$ must be the difference of the two terms on the right-hand side of Eq. (43). This results in the form:

$$C_2=\frac{1}{4}R^{1/2}(\infty)\lim_{x\to\infty}\{\exp[-\sigma_\infty x+H(x)]-f_{x0}\times\exp[-H(x)+H(\infty)]\};\quad \alpha_0<\alpha_\infty. \tag{47}$$

Now, the following specific convenient $\alpha_s(x)$ profile will be discussed:

$$\alpha_s(x)=\alpha_0\left(\frac{1+\Delta e^{-qx}}{1+\Delta}\right)^2;\quad \Delta\equiv\left(\frac{\alpha_0}{\alpha_\infty}\right)^{1/2}-1. \tag{48}$$

This is a decreasing profile ($\alpha_\infty<\alpha_0$) and Eq. (46) is appropriate. Upon taking the indicated limit:

$$\lim_{x\to\infty}\left(\sigma_\infty x-(1+i)(\omega/2)^{1/2}\int_0^x\frac{dx'}{\alpha_s^{1/2}(x')}\right)$$

$$=\sigma_\infty\lim_{x\to\infty}\left[x-\int_0^x\left(\frac{\alpha_\infty}{\alpha_s(x')}\right)^{1/2}dx'\right]=\sigma_\infty J, \tag{49}$$

where

$$J\equiv\int_0^\infty\left[1-\left(\frac{\alpha_\infty}{\alpha_s(x')}\right)^{1/2}\right]dx'=\frac{1}{2q}\ln(\alpha_0/\alpha_\infty). \tag{50}$$

Therefore,

$$C_2 = -\frac{R^{1/2}(\infty)}{4}(f_{\infty 0} + e^{-\sigma_\infty J}). \tag{51}$$

Since $\lim_{x\to\infty} H(x) = \infty$ for our choice of $\alpha_s(x)$, Eqs. (21), (42) and (51) yield

$$T(x) = -T_0\left(\frac{\sqrt{R(x)R(\infty)}}{4}\right)(f_{\infty 0} + e^{-\sigma_\infty J}) \times\{\exp[-2H(\infty) + H(x)] - \exp[-H(x)]\} \tag{52}$$

so that $T(0) = T_0(\omega)$ requires that

$$f_{\infty 0} = 4R^{1/2}(\infty), \tag{53}$$

where $f_{\infty 0}$ is fixed such that if $\alpha_s(x)$ is set equal to α_0, then $J \to \infty$, and the temperature becomes that of a homogeneous sample with thermal diffusivity α_0 throughout, as per Eq. (45).

Finally, the surface temperature can be written as

$$T(0;\omega,\alpha_0,\alpha_\infty) = T_0(\omega)\left\{1 + \frac{1}{4}R^{1/2}(\infty) \times\exp\left[-\frac{(1+i)\sqrt{\omega}}{2\sqrt{2q}}\frac{1}{\sqrt{\alpha_\infty}}\ln\left(\frac{\alpha_0}{\alpha_\infty}\right)\right]\right\}. \tag{54}$$

The following limits are easy to verify:

$$\lim_{\omega\to\infty} T(0) = T_0(\omega); \quad \text{(surface domination)}, \tag{55a}$$

$$\lim_{\omega\to 0} T(0) = T_0(\omega)\left(1 + \frac{1}{4}R^{1/2}(\infty)\right) > T_0(\omega); \quad \text{(bulk domination)}, \tag{55b}$$

$$\lim_{\alpha_\infty\to\alpha_0} T(0) = \lim_{q\to 0} T(0) = T_0(\omega); \quad \text{[homogeneous profile; } \alpha_s(x) = \alpha_0\text{]}. \tag{55c}$$

III. THE INVERSE PROBLEM AND $\alpha_s(x)$ PROFILE SIMULATIONS

In this section a versatile technique is presented, which reconstructs thermal diffusivity depth profiles quantitatively from the frequency responses of continuously inhomogeneous condensed phases, when normalized by the response of a homogeneous (reference) sample of temperature profile $T_0(\omega)$ given by Eqs. (28) and (45). The approach to the inverse problem, i.e., the $\alpha_s(x)$ reconstruction, depends on the incremental frequency dependence of the thermal-wave amplitude and phase and is directly adaptable to front-detection photothermal methods, ideally PAS.

We define the ratio of the continuously inhomogeneous temperatures $T(0)$, Eq. (54), to the homogeneous temperature T_0, Eq. (45):

$$M(\omega) \equiv T(0;\omega,\alpha_0,\alpha_\infty)/T_0(\omega). \tag{56}$$

Taking the case of a monotonically decreasing $\alpha_s(x)$ profile, the normalized thermal-wave signal corresponding to the profile (48) is given by

$$|M(\omega)|e^{i\Delta\phi(\omega)} = 1 + \frac{1}{4}R^{1/2}(\infty) \times\exp\left[-\frac{(1+i)\sqrt{\omega}}{2\sqrt{2q}}\frac{1}{\sqrt{\alpha_\infty}}\ln\left(\frac{\alpha_0}{\alpha_\infty}\right)\right], \tag{57}$$

where $|M(\omega)|$ is the amplitude ratio and $\Delta\phi(\omega)$ is the phase difference. In order to reconstruct the profile (48) with prior knowledge of the surface value α_0 (the same as that of the reference sample), one needs to calculate the parameters q and α_∞ from the data. Let

$$c \equiv \frac{1}{2q}\left(\frac{1}{2\alpha_\infty}\right)^{1/2}\ln\left(\frac{\alpha_0}{\alpha_\infty}\right). \tag{58}$$

Furthermore, from the definition of $R(x)$, Eq. (46b), assuming that the effusivity ratio at $x=\infty$ and $x=0$ is adequately represented by the respective conductivity ratio, one obtains

$$\alpha_\infty \approx \alpha_0/R^2(\infty). \tag{59}$$

The adequacy of this approximation was tested and found to be sufficient from the fidelity of numerically reconstructed $\alpha_s(x)$ profiles (see Sec. IV below).

The essence of our technique lies in its treatment of differential subsurface layers corresponding to a measurement at modulation frequency $f_j = \omega_j/2\pi$, with local $\alpha_s(x;f_j)$ values determined by redefining (updating) the values for c and $R(\infty)$ found at a neighboring modulation frequency $f_{j+1} = \omega_{j+1}/2\pi$, differing from f_j by $\delta f = f_{j+1} - f_j \ll f_j$. For small frequency decrements

$$\omega_{m-1} = \omega_m - \delta\omega; \quad \delta\omega \ll \omega_m \tag{60}$$

we can write to a high degree of accuracy:

$$\omega_{m-1}^{1/2} = \omega_m^{1/2}[1 - (\delta\omega/2\omega_m)]. \tag{61}$$

Separation of Eq. (57) in real and imaginary parts leads to the following exact expressions for the thermal-wave amplitude ratio and phase difference:

$$|M(\omega)|^2 = 1 + \tfrac{1}{2}R^{1/2}(\infty)e^{-c\sqrt{\omega}}\cos(c\sqrt{\omega}) + \tfrac{1}{16}R(\infty)e^{-2c\sqrt{\omega}} \tag{62a}$$

and

$$\Delta\phi(\omega) = -\tan^{-1}\left(\frac{\frac{1}{4}R^{1/2}(\infty)e^{-c\sqrt{\omega}}\sin(c\sqrt{\omega})}{1 + \frac{1}{4}R^{1/2}(\infty)e^{-c\sqrt{\omega}}\cos(c\sqrt{\omega})}\right). \tag{62b}$$

In addition, expansion of the exponential in Eq. (57) according to the approximation (61), evaluated at angular frequency $\omega_{m-1} < \omega_m$

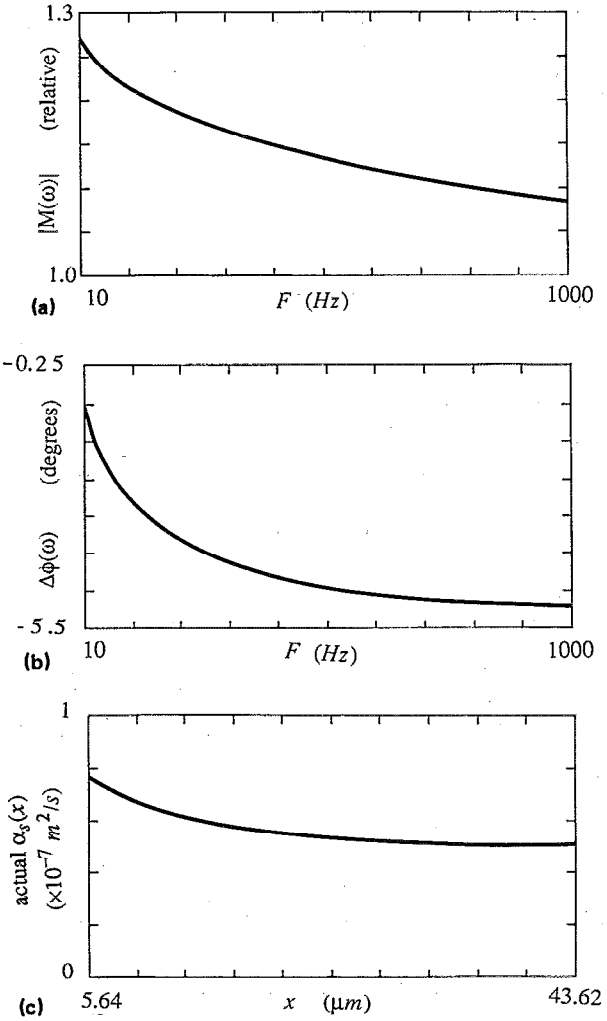

FIG. 1. (a) Amplitude ratio and (b) phase difference between a sample with $\alpha_0 = 1 \times 10^{-7}$ m^2/s, $\alpha_\infty = 5\times 10^{-8}$ m^2/s, $q = 10^5$ m^{-1}, [Eq. (48)], and a homogeneous reference with $\alpha_s = \alpha_0$. The thermal diffusivity profile is shown in (c). δf=0.1 Hz for this simulation.

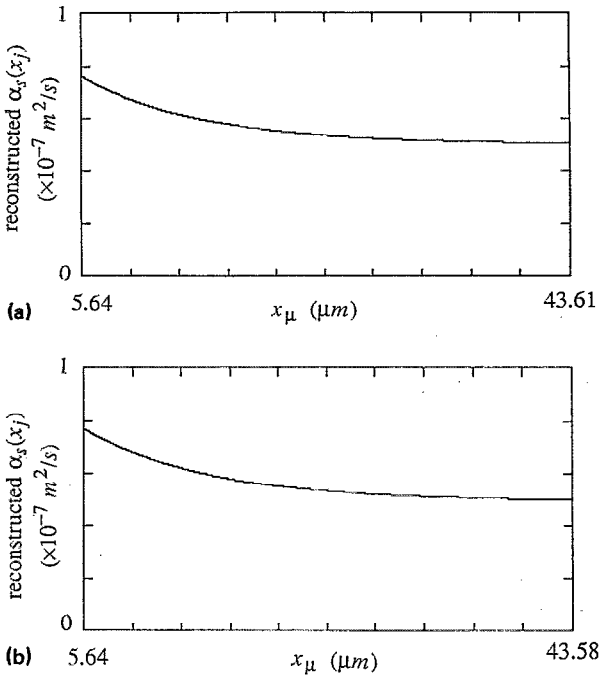

FIG. 2. Reconstruction of the thermal diffusivity profile from (a) amplitude data [Fig. 1(a)] and (b) phase data [Fig. 1(b)]; δf=0.1 Hz.

$$\exp[-(1+i)c\sqrt{\omega_{m-1}}] \approx \exp[-(1+i)c\sqrt{\omega_m}]\exp[(1+i)c\delta\omega/2\sqrt{\omega_m}], \tag{63}$$

gives a relation linking signals at the two neighboring frequencies ω_m and ω_{m-1}, when applied to Eq. (57) at $\omega = \omega_{m-1}$:

$$\exp(c_{m-1}\delta\omega/\sqrt{\omega_m}) = S^2(\omega_{m-1})/S^2(\omega_m), \tag{64}$$

where

$$S^2(\omega) \equiv |M(\omega)|^2 + 1 - 2|M(\omega)|\cos[\Delta\phi(\omega)]. \tag{65}$$

Therefore,

$$c_{m-1} = \left(\frac{2\sqrt{\omega_m}}{\delta\omega}\right)\ln\left(\frac{S(\omega_{m-1})}{S(\omega_m)}\right) \tag{66a}$$

$$= \frac{1}{2\sqrt{2}}\frac{\ln[\alpha_0/(\alpha_\infty)_{m-1}]}{q_{m-1}(\alpha_\infty)_{m-1}^{1/2}}. \tag{66b}$$

Equation (66a) can be used to determine c_{m-1}, i.e., the local value of c, from amplitude and phase data at frequencies ω_m and ω_{m-1}. Then, either Eq. (62a) or Eq. (62b) may be used at $\omega = \omega_{m-1}$ in order to determine the other unknown parameter $R(\infty)_{m-1}$. Once $R(\infty)$ is calculated, Eqs. (59) and (66b) evaluated locally at $\omega = \omega_{m-1}$ yield values for q_{m-1} and $(\alpha_\infty)_{m-1}$:

$$(\alpha_\infty)_{m-1} = \alpha_0/R^2(\infty)_{m-1} \tag{67a}$$

and

$$q_{m-1} = R(\infty)_{m-1}\ln[R(\infty)_{m-1}]/\sqrt{2\alpha_0}c_{m-1}. \tag{67b}$$

The versatility of the aforementioned technique lies in its ability to redefine the pair of values (q,α_∞) at every modulation frequency, which allows for local variations of $\alpha_s(x)$, as manifested by normalized experimental signal differences between neighboring frequencies. From this point of view, the original single exponential decay for $\alpha_s(x)$, Eq. (48) is solely used to supply local values for $(q,\alpha_\infty)\leftrightarrow\alpha_s(x_{\text{local}})$, and becomes irrelevant in the determination of the global depth profile, which is determined as an inverse problem from successive values of the entire set of the experimental data dependences on ω_j and can be any function of x, decreasing or increasing, numerical or in closed form. In the following simulations we test the fidelity of the reconstruction of a known $\alpha_s(x)$ depth profile from local values and, implicitly, the validity of the approximations (59) and (63). As a sample reference value α_0, a typical thermal diffusivity of the liquid crystal 4′-n-octyl-4-cyanobiphenyl (8CB) was chosen[18] in the nematic phase at ~37 °C:

$$\alpha_0 \approx \alpha_\parallel = 1\times 10^{-7}\ \text{m}^2/\text{s},$$

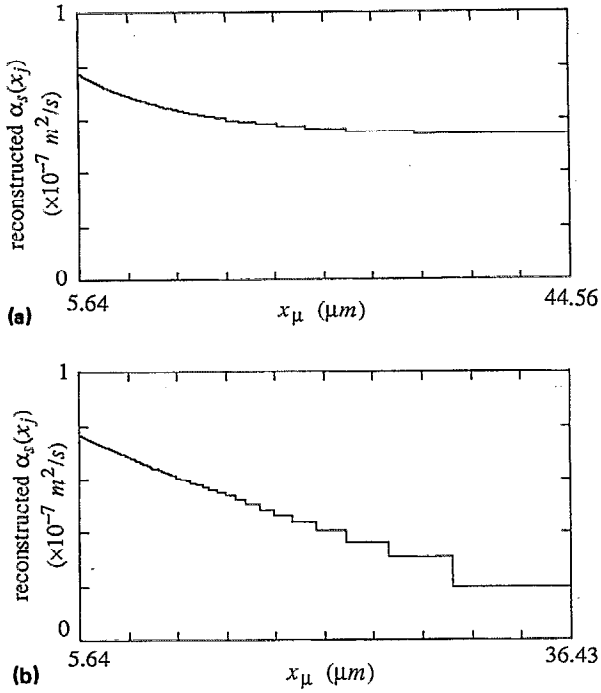

FIG. 3. Reconstruction of the thermal diffusivity profile from (a) amplitude data, [Fig. 1(a)] and (b) phase data, [Fig. 1(b)]; $\delta f = 10$ Hz.

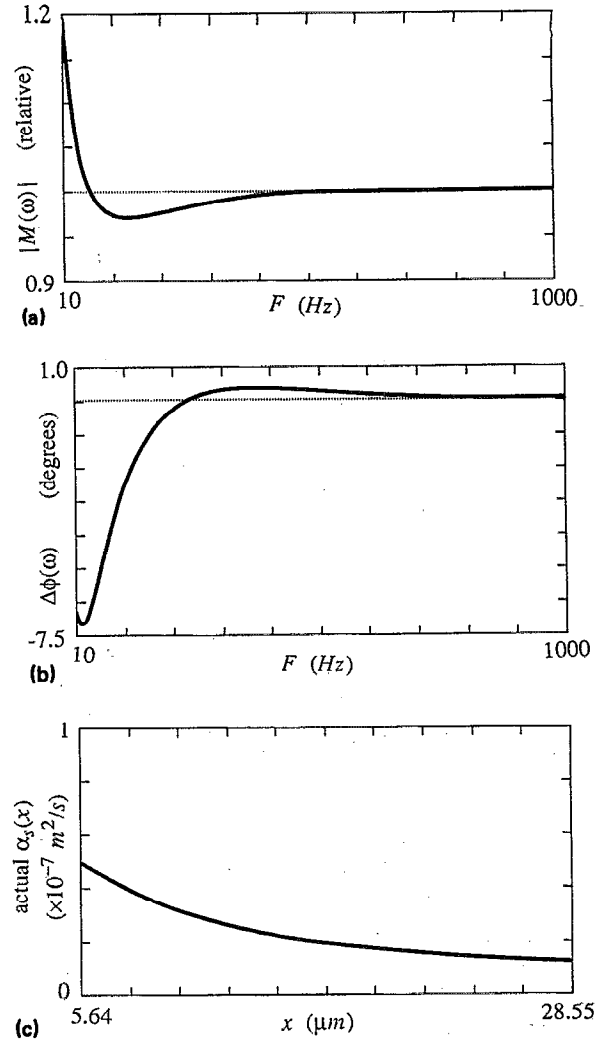

FIG. 4. (a) Amplitude ratio and (b) phase difference between a sample with $\alpha_0 = 1 \times 10^{-7}$ m^2/s, $\alpha_\infty = 1 \times 10^{-8}$ m^2/s, $q = 10^5$ m^{-1}, [Eq. (48)], and a homogeneous reference with $\alpha_s = \alpha_0$. The thermal diffusivity profile is shown in (c). $\delta f = 0.1$ Hz for this simulation.

where $\alpha_\parallel$ indicates a direction along the director of the liquid crystal.

Figure 1 shows the amplitude ratio $|M(\omega)|$ and phase difference $\Delta\phi(\omega)$ as a function of frequency, due to a hypothetical sample with thermal diffusivity profile given by Eq. (48) with

$$\alpha_0 = 1 \times 10^{-7} \text{m}^2/\text{s}, \quad \alpha_\infty = 5 \times 10^{-8} \text{ m}^2/\text{s},$$

and

$$q = 10^5 \text{ m}^{-1}.$$

These frequency responses were obtained using Eqs. (62a) and (62b) and the actual $\alpha_s(x)$ profile [Eq. (48)] is also shown. Then, using Eqs. (65)–(67) with $|M(\omega_j)|$ and $\Delta\phi(\omega_j)$ determined from the forward problem, with 1 kHz $\geqslant f_j \geqslant$ 10 Hz and $\delta_f = 0.1$ Hz, the inverse problem was solved and $\alpha_s(x)$ was reconstructed as shown in Fig. 2. It should be noticed that the $\alpha_s(x_j)$ obtained from the inverse problem, with either $R(\infty)$ from amplitude data, Fig. 2(a), or from $R(\infty)$ phase data, Fig. 2(b), is in excellent agreement with the original profile. The calculation of the depth parameter x_μ is performed based on the fact that as modulation frequency decreases, the thermal-wave probing depth (thermal diffusion length) $\mu_j = \mu(\omega_j)$ increases.[15] Starting the experiment at the highest practical frequency ω_n, i.e., the shortest $x_n \sim \mu_n$,[7] for $j = n$ we can write

$$x_n = \mu_n \equiv \Delta\mu_n = (2\alpha_0/\omega_n)^{1/2}, \tag{68}$$

where we approximate a surface slice with $\alpha_s(x) \approx \alpha_s(0) = \alpha_0$. The next (lower) modulation frequency, ω_{n-1}, corresponds to an increased thermal-wave depth:

$$x_{n-1} = \mu_{n-1} = \mu_n + \Delta\mu_{n-1}, \tag{69}$$

where μ_n is given by Eq. (68), and

$$\Delta\mu_{n-1} = (2\alpha_{n-1}/\omega_{n-1})^{1/2} - (2\alpha_{n-1}/\omega_n)^{1/2}, \tag{70}$$

and so on, for $x_{n-2}, x_{n-3}, \ldots, x_0$. As shown by comparison of the abscissas of Figs. 1(c) and 2, the above (approximate) calculation leads to a reproduction x_j of the actual depth parameter x better than 0.07%, which is the worst case resulting from the accumulated error at the lowest available frequency $f_0 = 10$ Hz. Figure 3 shows $\alpha_s(x_j)$ reconstructions from amplitude and phase data when $\delta f = 10$ Hz. Upon comparison with Fig. 1(c), we note that the fidelity of the amplitude-data reconstruction is still very high, except at the very lowest frequencies/greatest depths. On the other hand, the phase-data reconstruction appears to be poor throughout the entire frequency range. It is to be expected that as the condition $\delta\omega \ll \omega_m$ breaks down, the expansion Eq. (63) may no longer be valid. Figure 3 indicates that amplitude-data reconstructions may be more tolerant to the violation of this condition than phase-data reconstructions.

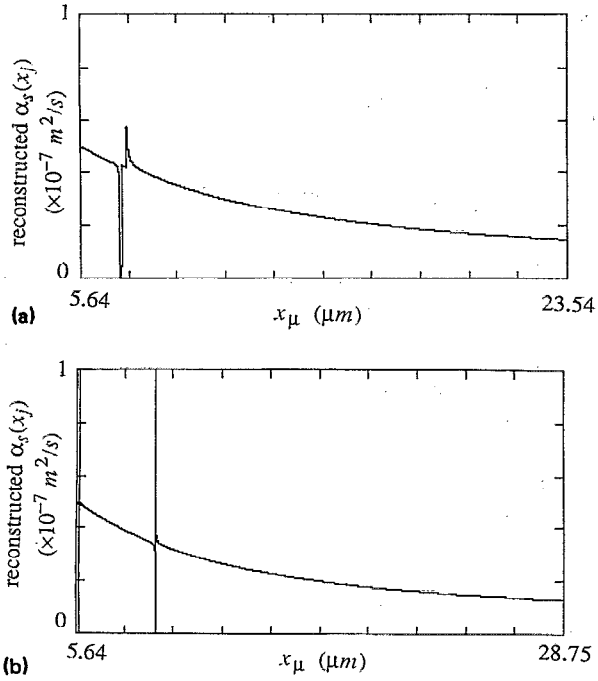

FIG. 5. Reconstruction of the thermal diffusivity profile from (a) amplitude data, [Fig. 4(a)] and (b) phase data, [Fig. 4(b)]; $\delta f = 0.1$ Hz.

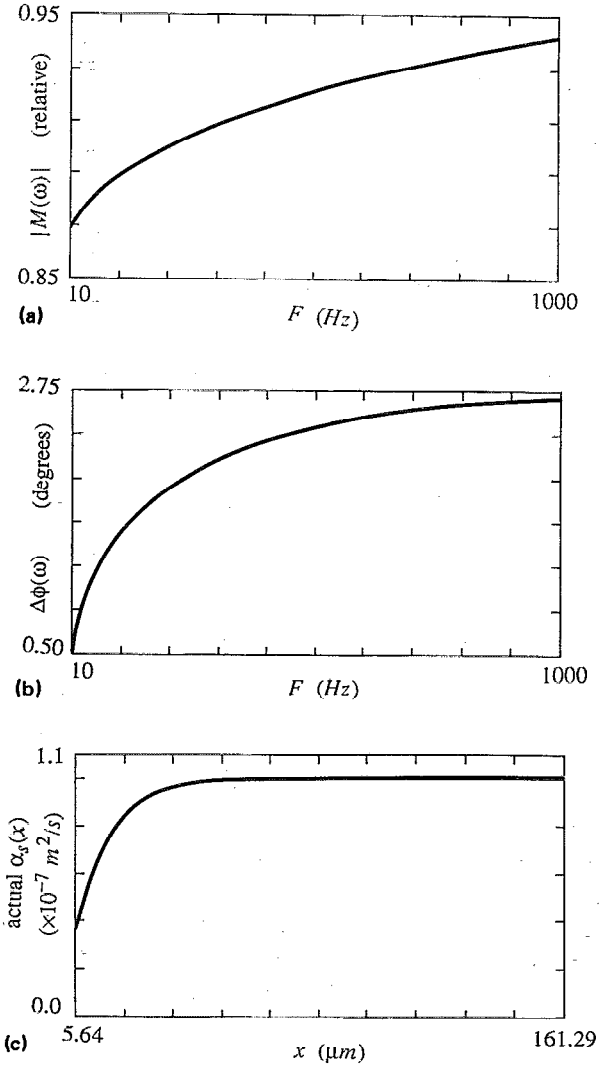

FIG. 6. (a) Amplitude ratio and (b) phase difference between a sample with $\alpha_0 = 1 \times 10^{-7}$ m^2/s, $\alpha_\infty = 1\times 10^{-6}$ m^2/s, $q = 10^5$ m^{-1}, [Eq. (71)], and a homogeneous reference with $\alpha_s = \alpha_0$. The thermal diffusivity profile is shown in (c). $\delta f = 0.1$ Hz for this simulation.

If a steeper decay of the thermal diffusivity profile is chosen, as in Fig. 4, the monotonic behavior of the frequency response in Fig. 1 is replaced by a more complicated behavior characterized by the appearance of extrema in both amplitude and phase. It is interesting to note that these features are qualitatively similar to plots of the surface temperature frequency response from a discrete two-layered solid, in the case where the thermal conductivity of the substrate is lower than that of the overlayer (Ref. 2, Fig. 4). We hypothesize that the steeper the $\alpha_s(x)$ decay, the closer the similarity of the continuously inhomogeneous sample to a step-functional distribution, as the limiting value α_∞ is reached at relatively shallower depths (higher frequencies). Figure 5 shows the reconstructed $\alpha_s(x_j)$ from both data channels. It was observed that at values of ω_j in the vicinity of zeros of the function $\tan\Delta\phi(\omega)$, Eq. (62b), or $|M(\omega)|=1$, Eq. (62a), discontinuities appear in the reconstructed profiles due to the indeterminacy of those equations. These anomalies are worse in the amplitude-data reconstruction and further simulations showed that they spread out over much of the profile as the $\delta\omega \ll \omega_m$ condition is relaxed. For $\delta f = 0.1$ Hz, the phase-data reconstruction is excellent.

Finally, we briefly examine the case of a monotonically increasing $\alpha_s(x)$ profile, such as the case

$$\alpha_s(x) = \alpha_0\left(\frac{1-\Delta e^{-qx}}{1-\Delta}\right)^2; \quad \Delta \equiv 1-\left(\frac{\alpha_0}{\alpha_\infty}\right)^{1/2}. \qquad (71)$$

This is an increasing and saturating profile ($\alpha_\infty > \alpha_0$).

Figure 6 shows the normalized amplitude and phase frequency response for such an $\alpha_s(x)$ profile obtained by an increasing and saturating depth dependence. Figure 7 shows reconstructions of the diffusivity profile from both amplitude and phase data. In this case, too, the quality and fidelity of the reconstruction is excellent for $\delta f = 0.1$ Hz. It is important to point out that Eqs. (57) and (62), which were derived for a decreasing $\alpha_s(x)$ depth profile, are capable of high fidelity reconstruction of general profiles, increasing or decreasing, due to the redefinition of reconstructed $\alpha_s(x; f_j)$ values locally, in terms of the actual experimental amplitude and phase profiles. Larger δf increments result in poorer $\alpha_s(x)$ reconstruction, with that from the phase data being more susceptible to distortions, especially at low frequencies/great depths. Steeper diffusivity profiles than that assumed in Fig. 6(c) lead to nonmonotonic signal behavior, qualitatively similar to a discrete two-layer model, with the underlayer being a better thermal conductor than the overlayer (Ref. 2, Fig. 3).

IV. CRITIQUE OF THE APPROXIMATIONS TO THE THEORY

The high fidelity of the diffusivity reconstructions for decreasing and increasing $\alpha_s(x)$ profiles is a strong indica-

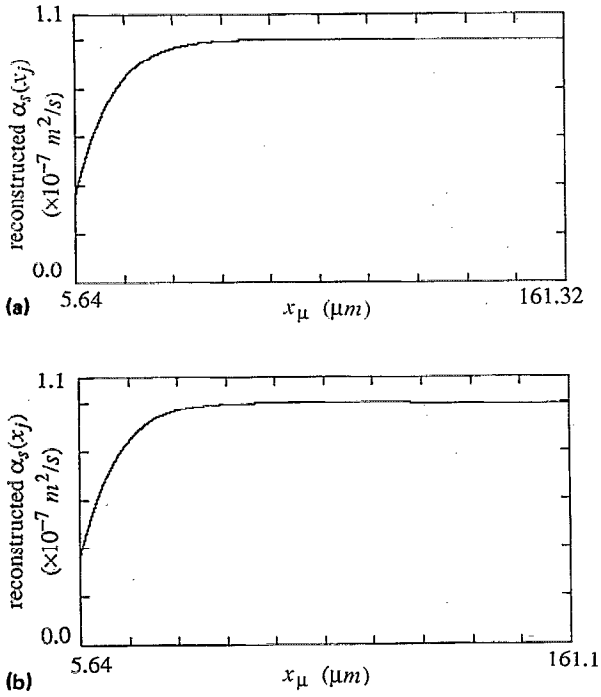

FIG. 7. Reconstruction of the thermal diffusivity profile from (a) amplitude data [Fig. 6(a)] and (b) phase data [Fig. 6(b)]; δf 0.1 Hz.

tion that the approximations Eqs. (59), (63) are valid throughout the tested frequency range. Approximation Eq. (59) implicitly assumes, in principle, the constancy of the heat capacity product $c(x)\,\rho(x)$ by equating its values at $x=0$ and $x=\infty$. In the actual application of the formula, however, its value is updated at every new frequency f_j, so that Eq. (59) becomes readjusted from data values. As a result the impact of the approximation is negligible. Approximation Eq. (63) is controllable by designing the experiment so that $\delta f \ll f_{\min}$, where $f_{\min} = f_0$ is the lowest usable frequency. In our simulations $\delta f/f_0 = 10^{-2}$ gave excellent reconstructions, whereas $\delta f/f_0 = 1$ resulted in poor fidelity at the deep end of the reconstructed $\alpha_s(x)$ profile, especially from phase data.

The only approximation in the formulation of the theoretical development leading to the key equations (41), (44) was Eq. (26), i.e., the assumed negligible contribution to the temperature profile from a term proportional to the spatial rate of change of the inverse square root of the thermal effusivity $e_s(x)$. If that term is included in the calculation of the heat flux, Eq. (41), an extra term will appear in the expression for $dT(x)/dx$:

$$T_s(0)e_s^{1/2}(0)\left(\frac{d}{dx}e_s^{-1/2}(x)\right)(C_1e^{H(x)} - C_2e^{-H(x)}).$$

Therefore, a comparison with Eq. (41) shows that the above term will be negligible only if and when

$$\frac{|\sigma(x)|}{e_s^{1/2}(x)} \gg \frac{d}{dx}e_s^{-1/2}(x). \tag{72}$$

Relation (72) amounts to comparing $[\omega/\alpha_s(x)]^{1/2}$ to $-(1/2)(d/dx)\ln[e_s(x)]$. Assuming that the heat capacity $\rho(x)c(x) \sim \rho(0)c(0)$, which was well justified from the fidelity of our simulations, we obtain:

$$-\frac{1}{2}\frac{d}{dx}\ln[e_s(x)] \approx -\frac{d}{dx}\ln[\alpha_s(x)]. \tag{73}$$

Using the decreasing $\alpha_s(x)$ profile, Eq. (48), the comparison to Rel. (72) amounts to comparing

$$\left(\frac{\omega}{\alpha_0}\right)^{1/2}\left(\frac{1+\Delta}{1+\Delta e^{-qx}}\right) \gg 2q\left(\frac{\Delta e^{-qx}}{1+\Delta e^{-qx}}\right). \tag{74}$$

Use of the definition of Δ, Eq. (48), yields the requirement

$$F_1(\omega) \gg F_2(x), \tag{75a}$$

where

$$F_1(\omega) \equiv \left(\frac{\omega}{\alpha_0}\right)(1+\Delta) = \left(\frac{\omega}{\alpha_\infty}\right)^{1/2} \tag{75b}$$

and

$$F_2(x) \equiv 2q\Delta e^{-qx}. \tag{75c}$$

Condition (75a) is always satisfied as $x \to \infty$, with worst case at $x=0$. To establish its general validity many computer simulations were performed with $q \to 0$, $q \to \infty$, $\alpha_\infty \to \alpha_0$, $\alpha_\infty \to 0$. In all cases, Rel. (75a) was always found to be satisfied, and within the frequency range 10 Hz$\leqslant f \leqslant$100 kHz. Figure 8 shows plots of our worst identified case, where $F_2(x)$ is relatively large. It can be seen that throughout the extended frequency range from 10 Hz to 100 kHz, $F_2(x)$ is always at least one order of magnitude smaller than F_1. We conclude from these considerations that our approximation Eq. (26) is definitely valid for all our reconstructions and thus the presented forward theory and inverse problem are internally consistent.

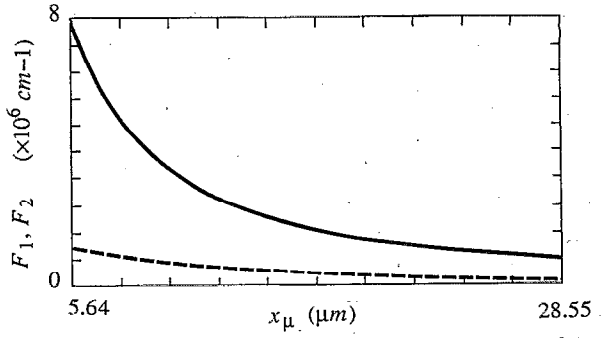

FIG. 8. Comparisons of magnitudes of $F_1(\omega)$, (75b), and $F_2(x)$, (75c) for thermal diffusivity parameters $\alpha_0 = 1 \times 10^{-7}$ m^2/s, $\alpha_\infty = 1\times 10^{-8}$ m^2/s, $q = 10^5$ m^{-1}, and 10 Hz $\leqslant f \leqslant$1 kHz. (F_1): solid line; (F_2): dashed line. Abscissas correspond to typical experimental depths in 8CB with frequency-to-depth conversions from Eq. (69).

V. CONCLUSIONS

The Hamilton–Jacobi formulation of the thermal-wave problem for a continuously inhomogeneous semifinite and optically opaque condensed phase specimen was found to provide a simple, well-defined, versatile and internally consistent method to approach the inverse problem of thermal

diffusivity depth profile reconstruction from both photoacoustic signal amplitude and phase channels. Increasing and decreasing diffusivity profiles in the value range of the liquid crystal 8CB were accurately reconstructed. The versatility of the reconstruction method lies in its ability for self-adjustment based on information in the actual experimental data. Many applications can be envisaged, such as with surface-treated materials, high-temperature and metal quenching processes, radiation damage in solids, etc. A first application to liquid crystals in the presence of an applied transverse magnetic field is presented elsewhere.[16]

ACKNOWLEDGMENTS

We wish to gratefully acknowledge the support of the Natural Sciences and Engineering Research Council of Canada (NSERC), of the Ontario Laser and Lightwave Research Center (OLLRC), and of the Research Council of the Katholieke Universiteit Leuven.

[1] S. D. Campbell, S. S. Yee, and M. A. Afromowitz, IEEE Trans. Biomed. Eng. **BME-26**, 220 (1979).
[2] J. Opsal and A. Rosencwaig, J. Appl. Phys. **53**, 4240 (1982).
[3] A. Mandelis and J. D. Lymer, Appl. Spectrosc. **39**, 473 (1985).
[4] J. Baumann and R. Tilgner, Can. J. Phys. **64**, 1291 (1986).
[5] A. Mandelis, Y. C. Teng, and B. S. H. Royce, J. Appl. Phys. **50**, 7138 (1979).
[6] M. A. Afromowitz, P-S. Yeh, and S. Yee, J. Appl. Phys. **48**, 209 (1977).
[7] A. Harata and T. Sawada, J. Appl. Phys. **65**, 959 (1989).
[8] A. K. S. Thakur, Lett. Heat Mass Transfer **9**, 385 (1982).
[9] V. L. Ginzburg, *Propagation of Electromagnetic Waves in Plasmas* (Pergamon, New York, 1971).
[10] V. Gusev, Ts. Velinov, and K. Bransalov, Semicond. Sci. Technol. **4**, 20 (1989).
[11] H. J. Vidberg, J. Jaarinen, and D. O. Riska, Can. J. Phys. **64**, 1178 (1986).
[12] J. Jaarinen and M. Luukkala, J. Phys. (Paris) **44**, C6-503 (1983).
[13] A. Mandelis, J. Math. Phys. **26**, 2676 (1985).
[14] H. Goldstein, *Classical Mechanics* (Addison-Wesley, Reading, MA, 1965), Chap. 9.
[15] A. Rosencwaig and A. Gersho, J. Appl. Phys. **47**, 64 (1976).
[16] A. Mandelis, E. Schoubs, S. Peralta, and J. Thoen, J. Appl. Phys. **70**, 1771 (1991).
[17] H. S. Carslaw and J. C. Jaeger, *Conduction of Heat in Solids* (Clarendon, Oxford, 1960), 2nd ed., Sec. 2.6.
[18] T. Akahane, M. Kondoh, K. Hashimoto, and M. Nakagawa, Jpn. J. Appl. Phys. **26**, L1000 (1987).